



LJMU Research Online

Israde-Alcántara, I, Domínguez-Vázquez, G, Gonzalez, S, Bischoff, J, West, A and Huddart, D

Five Younger Dryas black mats in Mexico and their stratigraphic and paleoenvironmental context

<http://researchonline.ljmu.ac.uk/id/eprint/6978/>

Article

Citation (please note it is advisable to refer to the publisher's version if you intend to cite from this work)

Israde-Alcántara, I, Domínguez-Vázquez, G, Gonzalez, S, Bischoff, J, West, A and Huddart, D (2017) Five Younger Dryas black mats in Mexico and their stratigraphic and paleoenvironmental context. Journal of Paleolimnology. ISSN 0921-2728

LJMU has developed [LJMU Research Online](#) for users to access the research output of the University more effectively. Copyright © and Moral Rights for the papers on this site are retained by the individual authors and/or other copyright owners. Users may download and/or print one copy of any article(s) in LJMU Research Online to facilitate their private study or for non-commercial research. You may not engage in further distribution of the material or use it for any profit-making activities or any commercial gain.

The version presented here may differ from the published version or from the version of the record. Please see the repository URL above for details on accessing the published version and note that access may require a subscription.

For more information please contact researchonline@ljmu.ac.uk

<http://researchonline.ljmu.ac.uk/>

2 **Five Younger Dryas black mats in Mexico and their**
3 **stratigraphic and paleoenvironmental context**

4 **Isabel Israde-Alcántara**  · **G. Domínguez-Vázquez** · **S. Gonzalez** ·
5 **J. Bischoff** · **A. West** · **D. Huddart**

6 Received: 12 March 2016 / Accepted: 8 June 2017
7 © Springer Science+Business Media B.V. 2017

8 **Abstract** The Younger Dryas interval (YD) was a
9 period of widespread, abrupt climate change that
10 occurred between 12,900 and 11,700 cal yr BP
11 (10,900–10,000 ¹⁴C BP). Many sites in the Northern
12 Hemisphere preserve a sedimentary record across the
13 onset of the YD interval, including sites investigated
14 in sedimentary basins located in central Mexico
15 (Chapala, Cuitzeo, Acambay), the Basin of Mexico
16 (Tocuila), and northern Mexico (El Cedral). Deposits
17 consist of lacustrine or marginal lake sediments that
18 were deposited during the Pleistocene and the
19 Holocene. At the Tocuila and Acambay sites, Pleis-
20 tocene fossil vertebrate assemblages, mainly mam-
21 moths (*Mammuthus columbi*), are found in association
22 with a distinctive organic layer, sometimes called the
23 black mat that formed during the YD. At the Chapala,
24 Cuitzeo, Acambay, and Tocuila sites the black mats

contain a suite of distinctive microscopic and miner- 25
alogical signatures and are accompanied by a sharp 26
change in the depositional environments as supported 27
by diatom and pollen studies reported here. The 28
signatures include magnetic, Fe-rich microspherules, 29
silica melted droplets with aerodynamic shapes (tek- 30
tites), large amounts of charcoal, and sometimes 31
nanodiamonds (Cuitzeo), all of which were deposited 32
at the onset of the YD. The geochemistry of the 33
microspherules indicates that they are not anthro- 34
pogenic, authigenic or of cosmic or volcanic origin, 35
and instead, were produced by melting and quenching 36
of terrestrial sediments. Here, we present the stratig- 37
raphy at five field sites, the analyses of magnetic 38
microspherules, including major element composition 39
and scanning electron microscopy images. All of these 40
materials are associated with charcoal and soot, which 41

A1 I. Israde-Alcántara (✉)
A2 Instituto de Ciencias de la Tierra, Universidad
A3 Michoacana de San Nicolás de Hidalgo, Morelia,
A4 Michoacán, Mexico
A5 e-mail: isaisrade@gmail.com

A6 G. Domínguez-Vázquez
A7 Faculty of Biology, Universidad Michoacana de San
A8 Nicolás de Hidalgo, Morelia, Michoacán, Mexico
A9 e-mail: gdoguez@yahoo.com.mx

A10 S. Gonzalez · D. Huddart
A11 School of Natural Sciences and Psychology, Liverpool
A12 John Moores University, Liverpool L3 3AF, UK
A13 e-mail: S.Gonzalez@ljmu.ac.uk

A14 D. Huddart
A15 e-mail: d.huddart@ljmu.ac.uk

A16 J. Bischoff
A17 Geochemistry, United States Geological Survey,
A18 Menlo Park, CA, USA
A19 e-mail: Jbischoff1@sbcglobal.net

A20 A. West
A21 GeoScience Consulting, Dewey, AZ 86327, USA
A22 e-mail: allen7633@aol.com

42 are distinctive stratigraphic markers for the YD layer
43 at several sites in Mexico.

44 **Keywords** Stratigraphy · Lacustrine · Magnetic
45 microspherules · Abrupt change in
46 paleoenvironments · Charcoal

47 Introduction

48 The Younger Dryas boundary (YDB) impact hypoth-
49 esis proposes that multiple extraterrestrial impactors
50 collided with the Earth at ~12,900 cal yr BP. One
51 impactor either exploded above or on the Laurentide
52 ice sheet causing destabilization of the ice sheet. It is
53 proposed that the impacts occurred over a short span of
54 a few days or less, affecting parts of four continents
55 (Firestone et al. 2007). The impact triggered extensive
56 biomass burning coeval with YD climate change
57 (Kennett et al. 2015), an abrupt cooling from ~12,900
58 to 11,700 cal yr BP, in which temperatures almost
59 returned to ice age conditions in several parts of the
60 world, including Europe, eastern North America, and
61 Mongolia (Carlson et al. 2007; Choi et al. 2014).
62 Firestone et al. (2007) further suggested that the YD
63 climate episode is associated with declines/reorgani-
64 zations of human populations in North America,
65 coincident with the mass extinction of 35 species of
66 vertebrates, mainly megafauna, such as mammoths,
67 camels, mastodonts and sabre-toothed cats.

68 These impacts deposited impact-related proxies,
69 including highly ornamented magnetic micro-
70 spherules, high-temperature meltglass (tektites), car-
71 bon spherules, glass-like carbon, aciniform carbon
72 (soot), and nanodiamonds (Firestone et al. 2007; Tian
73 et al. 2011; Bunch et al. 2012; Kinzie et al. 2014;
74 Wittke et al. 2013). Many of the YDB sites previously
75 studied were dated to approximately 12,900 cal yr BP
76 (Kurbatov et al. 2010; Kennett et al. 2015). The impact
77 hypothesis has generated heated opposition and crit-
78 icism. Some of the criticism is focused on the age
79 uncertainty of this proposed event (Meltzer et al.
80 2014). In order to calculate the most precise age
81 possible, Kennett et al. (2015) performed Bayesian
82 analyses, using the IntCal-13 calibration curve for 354
83 radiocarbon dates from 23 different stratigraphic
84 sections in 12 countries. This study showed that the
85 age of the YDB event falls between 12,835 and

12,735 cal yr BP (10.9 ¹⁴C ka BP radiocarbon years) 86
at a 95% probability, and this age coincides with the 87
onset of the YD cooling episode (Kennett et al. 2015). 88

89 However, Cooper et al. (2015) propose that a pre-
90 YD warming episode led to the demise of the
91 megafauna. On the other hand, it was proposed that
92 the disruptions both in human and animal populations
93 were likely due to impactors that produced extensive
94 fires and clouds of atmospheric dust and soot, resulting
95 in a decreased insolation that severely affected
96 photosynthesis (Firestone et al. 2007). At many of
97 the YD-age sites investigated, the reorganization/
98 decline in human populations and megafaunal extinc-
99 tions are proposed to have occurred immediately
100 before the deposition of a dark organic-rich sedimen-
101 tary layer, sometimes called a “black mat,” suggesting
102 a strong correlation of the black mat layer with
103 wildfires and climate change (Firestone et al. 2007).
104 For example, at several Clovis Palaeoindian sites in
105 the USA (Murray Springs, Arizona; Blackwater Draw,
106 New Mexico; and Topper, South Carolina) (Fig. 1),
107 the black mat forms a distinctive stratigraphic marker
108 at the onset of the YD climate change and is marked by
109 peak abundances of charcoal fragments from a major
110 episode of biomass burning. Holliday (1985) and
111 Quade et al. (1998) initially described the black mats
112 as sapropels and Scott et al. (2010) suggested that the
113 black mats are associated with algal blooms and fungi.
114 Similarly, Haynes (2008) interpreted the black mats as
115 resulting from algal production related to swampy,
116 high spring discharge and a high water table under
117 cold and humid conditions. More recently, Harris
118 Parks (2016) studied 25 different black mats in
119 Arizona, New Mexico, Texas, and Nevada, conclud-
120 ing that the organic matter found in the layers was
121 derived from herbaceous taxa.

122 Although some black mats, especially those in
123 northern Europe, are associated with wildfires (Fire-
124 stone et al. 2007), most researchers agree that some
125 black mats formed primarily because of major envi-
126 ronmental changes that occurred at the beginning of
127 the YD cooling episode, which resulted in major
128 changes in atmospheric and oceanic circulation pat-
129 terns (Firestone et al. 2007). The most widely accepted
130 explanation is that the YD climate change resulted
131 from the alteration of oceanic circulation by a massive
132 meltwater pulse into the Arctic Ocean (Tarasov and
133 Peltier 2005; Carlson et al. 2007; Carlson 2010;
134 Renssen et al. 2015) that triggered the shutdown of the

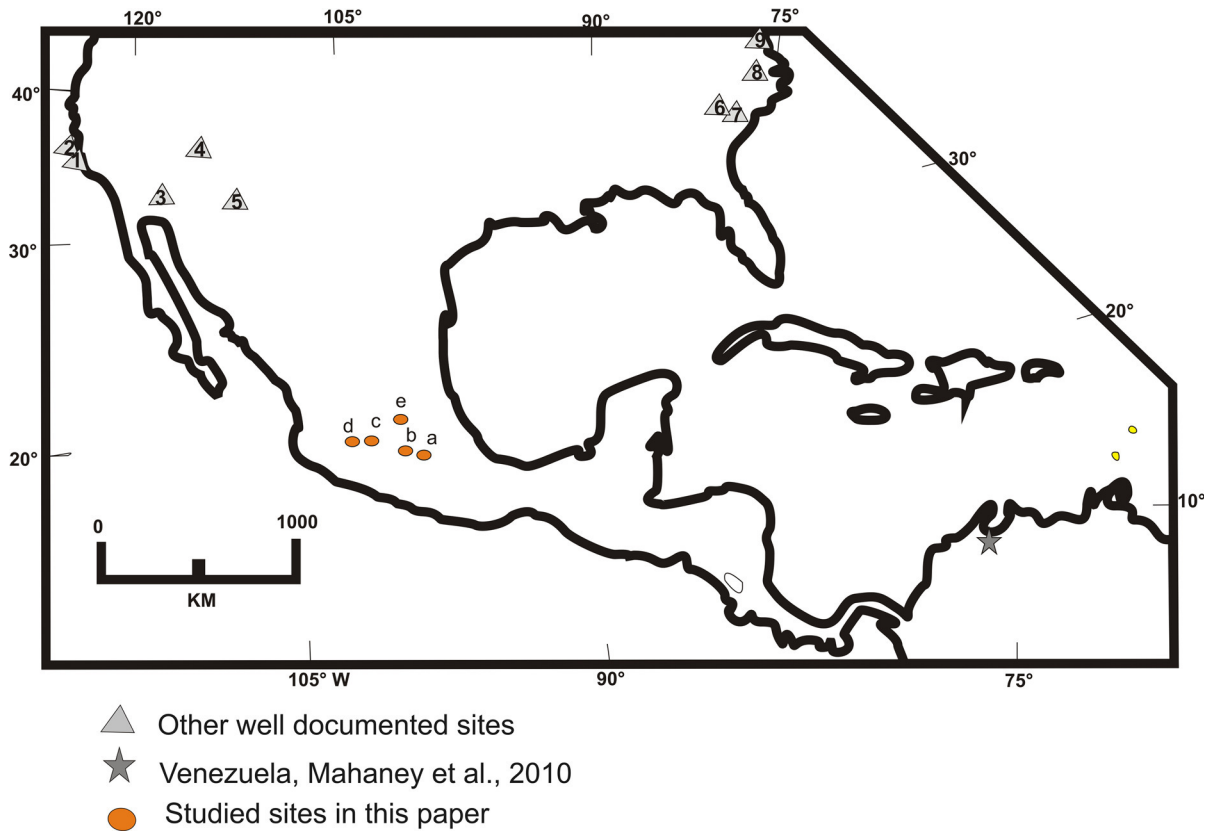


Fig. 1 Location of Mexican studied sites: (a) Tocuila, (b) Lake Acambay, (c) Lake Cuitzeo, (d) Lake Chapala, (e) El Cedral. Also in triangles are shown the locations of several YD sites from USA: (1) Daisy Cave, California; (2) Arlington Canyon,

California; (3) Murray Springs, Arizona; (4) Lindenmeir, Colorado; (5) Bull Creek, Oklahoma; (6) Blackville, South Carolina; (7) Topper, South Carolina; (8) Kimbel Bay, North Carolina; (9) Newtonville, New Jersey

135 Atlantic Meridional Overturning Circulation
 136 (AMOC). Alternatively, some researchers propose
 137 that YD climate change was produced by an unusual
 138 combination of different processes, such as an
 139 increased atmospheric dust load, due to reduction in
 140 atmospheric levels of methane and nitrous oxide
 141 (Renssen et al. 2015). Firestone et al. (2007) added an
 142 additional component by proposing that an extrater-
 143 restrial impactor triggered the meltwater flooding that,
 144 in turn, resulted in the shutdown of the AMOC, which
 145 initiated the YD cooling episode.

146 European and North American YD-age black mat
 147 deposits are nearly always associated with a diverse
 148 assemblage of unusual, impact-related proxies,
 149 including Fe-rich, dendritic microspherules, high-
 150 temperature meltglass, nanodiamonds, iridium, plat-
 151 inum, osmium, along with charcoal and burnt
 152 biomass. This association led Firestone et al. (2007)

to suggest that the formation of the black mats at
 12,900 cal yr BP resulted from the YDB impact
 event that triggered abrupt YD climate change that,
 in turn, produced widespread environmental change and
 extensive wildfires. Alternatively, some researchers
 (Haynes 2008; Scott et al. 2010) suggested that YDB
 microspherules are associated with volcanic ash or
 are simply produced due to the normal, daily influx of
 meteoritic debris. However, Wittke et al. (2013)
 demonstrated that the composition of YDB spherules
 is inconsistent with a volcanic or meteoritic origin,
 and instead, they appear to result from surficial
 terrestrial sediments that were melted by the extrater-
 restrial impacts. Israde-Alcántara et al. (2012) and
 LeCompte et al. (2012) have demonstrated that
 spherules are present only in the YDB strata and do
 not occur in sediments above or below, supporting an
 impact-related origin.

153
154
155
156
157
158
159
160
161
162
163
164
165
166
167
168
169
170

171 Similar climatic and associated sedimentation
 172 changes, along with impact-related proxies, such as
 173 melted microspherules, have been observed at the time
 174 of the YD in stratigraphic sections at nearly 40 sites
 175 across five different continents, mainly in the Northern
 176 Hemisphere. These include sites in the USA (Firestone
 177 et al. 2007; Kennett et al. 2009) (Fig. 1), Europe
 178 (Andronikov et al. 2011), east Asia (Andronikov et al.
 179 2013), Greenland (Kurbatov et al. 2010), Venezuela
 180 (Mahaney et al. 2010a, b), and in lake sediments from
 181 Lake Cuitzeo in Mexico (Israde-Alcántara et al. 2012).
 182 The Pleistocene–Holocene boundary has been identi-
 183 fied in several lakes in Central America, including
 184 Lake Peten Itza (Bush et al. 2009), La Chonta Bog in
 185 Costa Rica (Islebe and Hooghiemstra 2006) and Lake
 186 Chalco in central Mexico (Lozano García and Ortega
 187 Guerrero 1994). All the lakes show a warm Bølling-
 188 Allerød interstadial (pre-12,900 cal yr BP) with a
 189 cooler YD (12,900 to 11,500 cal yr BP), followed by a
 190 warm interval from 11,500 cal yr BP to the present. In
 191 these lakes the two peaks in pollen that bracket the YD
 192 with the presence of *Alnus*, *Quercus* and *Pinus* were
 193 observed. All these records indicate higher lake levels
 194 during the YD.

195 At Lake Chalco, forest pollen almost disappeared
 196 during the YD and was only observed at the end of YD
 197 interval (Lozano García and Ortega Guerrero 1994). A
 198 similar behavior was observed at Lake Cuitzeo
 199 (Fig. 1). In other neighbouring lakes inside the
 200 Chapala graben, further detailed sampling is needed
 201 to find YDB proxies. Correlation of the YD with other
 202 lake records is sometimes difficult because the sedi-
 203 ments are disturbed by tectonism or bioturbation.

204 A 6.61 m long littoral core was collected from the
 205 littoral zone of Lake Zirahuén (Ortega et al. 2010). At
 206 3.73 m depth, with a date of $10,290 \pm 60 \text{ C}^{14} \text{ yr BP}$, it
 207 is evident that there is a sharp irregular contact
 208 overlying laminated ooze with gray laminae contain-
 209 ing epiphytic taxa (*Cocconeis placentula*). Overlying
 210 this deposit, in discordance, an organic-rich, sandy silt
 211 shows an isolated peak of magnetic susceptibility. In
 212 these organic-rich, sandy silts, diatoms change to a
 213 planktonic community dominated by *Aulacoseira*
 214 *ambigua* indicating an abrupt change in sedimentation
 215 and in the diatom associations with more turbid and
 216 wetter conditions (slightly higher lake levels) than
 217 previously. A characteristic algal bloom represented
 218 by a *Pediastrum* increase and the disappearance of the
 219 fern, *Isoetes* in the same interval (at 3.73 m depth)

220 indicates an ecological reorganization at the Pleis-
 221 tocene–Holocene boundary (Torres-Rodríguez et al.
 222 2012).

223 In the Zacapu lake basin, west of Lake Cuitzeo, a
 224 trend to dry conditions during the late Pleistocene is
 225 interrupted by a 10 cm thick tephra interlayered with
 226 clays dated to 9750 C14 yr BP. In these strata, a peak
 227 of magnetic susceptibility has a positive correlation
 228 with high percentages of Total Organic Carbon (TOC)
 229 that are interpreted as an episode of humidity (Ortega
 230 et al. 2002). Further detailed sampling is needed to
 231 locate YDB proxies at this site.

232 Anomalous organic-rich black mat layers, often
 233 containing proxies of biomass burning, such as peak
 234 concentrations in charcoal and soot, have been found in
 235 several lacustrine basins in Mexico (Israde-Alcántara
 236 et al. 2012). Ornamented Fe-rich microspherules have
 237 been found at the Pleistocene–Holocene boundary at
 238 several of these sites. This study examines YD black
 239 mat layers and the characteristics of magnetic
 240 spherules found at several sites in Mexico.

241 Objectives

242 The general objective was to reconstruct the stratig-
 243 raphy and paleoenvironments during the Pleistocene/
 244 Holocene transition at five sites in Mexico. Some sites
 245 contained megafaunal remains in marginal lake
 246 deposits, as at the Tocuila and Acambay sites. In
 247 particular, it was attempted to identify the presence of
 248 YD sediment layers and to study their characteristics,
 249 particularly the record of diatoms, pollen, soot and
 250 magnetic spherules. These sites are associated with
 251 paleolakes or recently drained lakes (Fig. 1) and
 252 include: (a) Tocuila lake margin; (b) Lake Acambay,
 253 (c) Lake Cuitzeo; (d) Lake Chapala, (e) El Cedral
 254 springs/marshes. The stratigraphy and reconstruction
 255 of the paleoenvironment were investigated across the
 256 boundary between the late Pleistocene and early
 257 Holocene.

258 Methodology

259 Field outcrops (trenches) were cleaned using a shovel
 260 and trowel at the Tocuila and El Cedral sites, sampling
 261 sediments every 20 cm or where changes in sedimen-
 262 tation occurred.

Editor Proof

263 264 265 266 267 268 269 270 271	At Lake Acambay and Lake Cuitzeo cores were acquired using a long-gear coring system using pneumatic pressure, at 1 m intervals. At Lake Chapala a Usinger piston coring system was used. All the sediment cores were sampled every 10 cm. The Acambay and Cuitzeo cores are stored in refrigeration at the University Michoacana and the Chapala core is under refrigeration at the University of Guadalajara (Fig. 1).	306 307 308 309 310 311 312
272	Stratigraphy	
273 274 275 276 277	The description of the stratigraphic sequence and type of sediments in both field outcrops and lake cores was made with special emphasis on the late Pleistocene and early Holocene sediments, especially before, during, and after the YD transition.	313 314 315 316 317 318 319 320 321 322 323
278	Radiocarbon dating	
279 280 281 282 283 284 285 286 287 288 289 290 291 292 293 294 295 296	Samples were selected for ¹⁴ C AMS radiocarbon dating based on high TOC values in sediment cores, or by sampling visible charcoal levels, charcoal fragments or mollusc layers in field outcrops. The AMS radiocarbon dates were obtained from the National Ocean Sciences Accelerator Mass Spectrometry (NOSAMS) facility at Woods Hole (Massachusetts); Beta Analytic Laboratories (Miami); Oxford Radiocarbon Facility, UK and the Geochronology Laboratory of the National Taiwan University. The results were calibrated using the OxCal (version 4.2) (Bronk-Ramsey 2005) with the IntCal-13 calibration curve (Bronk-Ramsey 2009). All dates are expressed in radiocarbon years (¹⁴ C BP), calendar years before present (cal yr BP), or thousands of calibrated years BP (ka BP), depending on the previously published dates. In the text, we mostly use uncalibrated radiocarbon dates (¹⁴ C BP), but their calibrated equivalents are included in Table 1.	324 325 326 327 328 329 330 331 332 333 334 335 336 337 338 339
297	Microspherule analysis	
298 299 300 301 302 303 304 305	Using a strong, neodymium magnet, Fe-rich magnetic grains were isolated from a slurry prepared from sediments following the technique developed by Israde-Alcántara et al. (2012). Afterwards, those magnetic particles were wet sieved using sieves from >150 to >53 μm that were visually screened, hand-picked, and observed under a binocular zoom stereomicroscope. Carbon spherules were also extracted	340 341 342 343 344 345 346 347 348
	from a sediment slurry by flotation and hand picked for investigation. After selection, the magnetic microspherules and carbon spherules were fixed to SEM stubs for observation and analysis by energy-dispersive X-ray spectroscopy (EDS) undertaken on a JEOL JSM-6480LV scanning electron microscope using standard analytical techniques.	349 350 351 352 353 354 355 356 357 358 359 360 361 362 363 364 365 366 367 368 369 370 371 372 373 374 375 376 377 378 379 380 381 382 383 384 385 386 387 388 389 390 391 392 393 394 395 396 397 398 399 400 401 402 403 404 405 406 407 408 409 410 411 412 413 414 415 416 417 418 419 420 421 422 423 424 425 426 427 428 429 430 431 432 433 434 435 436 437 438 439 440 441 442 443 444 445 446 447 448 449 450 451 452 453 454 455 456 457 458 459 460 461 462 463 464 465 466 467 468 469 470 471 472 473 474 475 476 477 478 479 480 481 482 483 484 485 486 487 488 489 490 491 492 493 494 495 496 497 498 499 500 501 502 503 504 505 506 507 508 509 510 511 512 513 514 515 516 517 518 519 520 521 522 523 524 525 526 527 528 529 530 531 532 533 534 535 536 537 538 539 540 541 542 543 544 545 546 547 548 549 550 551 552 553 554 555 556 557 558 559 560 561 562 563 564 565 566 567 568 569 570 571 572 573 574 575 576 577 578 579 580 581 582 583 584 585 586 587 588 589 590 591 592 593 594 595 596 597 598 599 600 601 602 603 604 605 606 607 608 609 610 611 612 613 614 615 616 617 618 619 620 621 622 623 624 625 626 627 628 629 630 631 632 633 634 635 636 637 638 639 640 641 642 643 644 645 646 647 648 649 650 651 652 653 654 655 656 657 658 659 660 661 662 663 664 665 666 667 668 669 670 671 672 673 674 675 676 677 678 679 680 681 682 683 684 685 686 687 688 689 690 691 692 693 694 695 696 697 698 699 700 701 702 703 704 705 706 707 708 709 710 711 712 713 714 715 716 717 718 719 720 721 722 723 724 725 726 727 728 729 730 731 732 733 734 735 736 737 738 739 740 741 742 743 744 745 746 747 748 749 750 751 752 753 754 755 756 757 758 759 760 761 762 763 764 765 766 767 768 769 770 771 772 773 774 775 776 777 778 779 780 781 782 783 784 785 786 787 788 789 790 791 792 793 794 795 796 797 798 799 800 801 802 803 804 805 806 807 808 809 810 811 812 813 814 815 816 817 818 819 820 821 822 823 824 825 826 827 828 829 830 831 832 833 834 835 836 837 838 839 840 841 842 843 844 845 846 847 848 849 850 851 852 853 854 855 856 857 858 859 860 861 862 863 864 865 866 867 868 869 870 871 872 873 874 875 876 877 878 879 880 881 882 883 884 885 886 887 888 889 890 891 892 893 894 895 896 897 898 899 900 901 902 903 904 905 906 907 908 909 910 911 912 913 914 915 916 917 918 919 920 921 922 923 924 925 926 927 928 929 930 931 932 933 934 935 936 937 938 939 940 941 942 943 944 945 946 947 948 949 950 951 952 953 954 955 956 957 958 959 960 961 962 963 964 965 966 967 968 969 970 971 972 973 974 975 976 977 978 979 980 981 982 983 984 985 986 987 988 989 990 991 992 993 994 995 996 997 998 999 1000
	Organic material	313
	In the black sediments Total Organic Carbon (TOC) was determined with a UIC S014 coulometer coupled to a CM 5130 acidification module, based on the titration of a solution containing the CO ₂ produced by the calcination of sediments. Samples were crushed and 0.025 g of sediment was weighed, then placed on sterilized ceramic trays and dried in an oven. The percentage of organic carbon (TOC) was estimated by subtracting the TIC from the percentage of total carbon (TC) in each sample.	314 315 316 317 318 319 320 321 322 323
	Pollen analysis	324
	1 cm ³ sediment samples were processed using routine pollen techniques (Faegri and Iversen 1989), using HCl, KOH, HF, and acetolysis to digest the samples. A minimum of 100 pollen grains was counted for each sample when possible because the samples contained few pollen grains in general. Only taxa with abundances >5% were plotted in the pollen diagrams. For Cuitzeo we displayed the pollen graph in grains/gm of sediment in order to compare with the number of spherules per gram of sediment. For this we weighed one cm ³ of sediment to prepare the pollen samples. We expressed the number of grains/gm of sediment. Pollen diagrams are reported for the Tocuila and Cuitzeo sites, but the El Cedral site had very few pollen grains preserved, so a full count was not possible.	325 326 327 328 329 330 331 332 333 334 335 336 337 338 339
	Diatoms	340
	Sediments were sampled for diatoms, taking a 1 cm ³ every 10 cm at all sites, except at Tocuila, which was sampled every 20 cm. Each sample of 0.5 g of dried, bulk material was boiled in 30% hydrochloric acid at 100 °C to remove carbonates and repeated with hydrogen peroxide to eliminate organic matter. Samples were rinsed with distilled water until a neutral pH was reached. It was not necessary to use nitric acid to	341 342 343 344 345 346 347 348

Table 1 Studied sites characteristics and radiocarbon dates (uncalibrated and calibrated using OxCal 4.2, IntCal-13 curve after Bronk-Ramsey 2009)

Field sites	State	Latitude	Longitude	Altitude (m)	Geological setting	Spherule or soot	Biological key material	System	¹⁴ C yrs BP ^a	IntCal-13 BP 95% prob
Cuitzeo	Michoacán	19°53'15"	100°50'20"	1924	Lake	Spherule	Diatoms Charcoal Organic sediments	Lacustrine	8830 ± 215 10,550 ± 35 29,870 ± 100	10,486 to 9519 12,680 to 12,471 28,218 to 27,742
Chapala	Jalisco	20°17'36"	103°15'08"	1528	Lake	Spherule	Diatoms Charcoal	Lacustrine	12,560 ± 50	15,193 to 14,580
Tocuila (Texcoco)	Estado de México	19°31'23"	98°58'49"	2240	Lake, shoreline	Spherule	Pollen diatoms Charcoal	Lacustrine	10,016 ± 39 10,800 ± 50	11,313 to 11,121 15,193 to 14,580
Acambay	Estado de México	19°56'17"	99°52'46"	2533	Lake	Spherule	Diatoms Mamuth Pollen	Lacustrine	8510 ± 40 12,100 ± 65 16,296 ± 517	9594 to 9521 14,176 to 13,821 21,081 to 16,628
El Cedral	San Luis Potosí	23°48'35"	100°44'03"	1702	Pond/Spring hydrothermal	Soot	Pollen	Lacustrine	8520 ± 40 9360 ± 40 10,350 ± 40	9540 to 9470 10,690 to 10,500 12,390 to 12050

The radiocarbon dates in bold highlight dates for the organic-rich black mat layers at the sites that were produced during the YD interval. All contain magnetic Fe-rich microspherules and carbon microspherules, except for the El Cedral site

^a Radiocarbon dates in bold are related to Younger Dryas interval

354 obtain cleaned frustules. Samples were mounted on
 355 coverslips using Naphrax (refraction index = 1.7).
 356 Diatoms were identified using an Olympus Bymax 50
 357 light microscope at a magnification of 1000x. Taxo-
 358 nomic identification was based on Krammer and
 359 Lange Bertalot (1997a, b, 2004), and was compared
 360 with previous studies of Mexican taxonomy (Israde-
 361 Alcántara et al. 2010; Almanza Alvarez et al. 2016).
 362 Generally, a minimum of 400 diatoms were counted
 363 per slide, except when there were insufficient num-
 364 bers, in which case, at least 200 diatoms were counted
 365 per slide (Battarbee et al. 2001). Frustules were
 366 counted only when more than a half of the frustule
 367 was clearly identifiable and expressed as percentage
 368 values. The main representative taxa are shown in the
 369 diagrams with an abundance of >5%. Diatoms were
 370 not preserved at the El Cedral site.

371 Results

372 Stratigraphy and paleoenvironments

373 Five studied sites in Mexico included lacustrine and
 374 nearshore lake margins (Fig. 1) with altitudes varying
 375 from 1528 m a.s.l. at Lake Chapala to 2533 m a.s.l. at
 376 the drained, marshy Lake Acambay. In Fig. 2, the
 377 stratigraphic sequences and thicknesses for each layer
 378 are shown. The sites are mainly located in the Trans-
 379 Mexican Volcanic Belt (TMVB), which formed as a
 380 result of subduction of the Cocos and Rivera Plates
 381 under the North American Plate and a NE-SW and an
 382 E-W preferential fault and fracture system has devel-
 383 oped since the Miocene that produced calcalkaline
 384 volcanism (De Mets and Stein 1990) and a series of
 385 lacustrine basins aligned along the graben in west
 386 central Mexico (Israde-Alcántara et al. 2010). Only
 387 the El Cedral site is located on the Central High
 388 Plateau in Mexico at its boundary with the TMVB.

389 The stratigraphy at each of the sites ca. 1 m before
 390 and 1 m after the YD is described, including the main
 391 pollen and diatom taxa. In Fig. 2, the stratigraphic
 392 sequences and thicknesses for each layer are shown.

393 *Tocuila*

394 The Tocuila site, rich in mammoth fossils is located
 395 close to a former shoreline of Lake Texcoco in the
 396 state of Mexico. The site was originally excavated and

studied by Morett et al. (1998). Subsequently, Siebe 397
 et al. (1999), González and Huddart (2007) and 398
 González et al. (2014) discussed the stratigraphy, 399
 mammoth fossils, tephra, lahars and the diatom and 400
 pollen record at this site. The original excavation 401
 trench has been converted into an in situ museum, 402
 where it is possible to observe a channel infilled by a 403
 lahar derived from the Upper Toluca Pumice (UTP), a 404
 tephra marker for the Basin of Mexico. At least seven 405
 mammoths were found embedded in this lahar. The 406
 lake sediment sequence preceding the lahar can be 407
 observed in the north wall of the field museum (see 408
 Fig. 2a). The base of the sequence consists of black, 409
 basaltic ashfall (Sample 1), correlated with the Great 410
 Basaltic Ash and dated by Mooser (1967) to 411
 $28,600 \pm 200$ ^{14}C BP. This stratum is overlain by 412
 oxidized sandy silt covered by a fine sand layer 413
 containing several bone fragments. Toward the top, 414
 the sediments become sandier and are covered by an 415
 irregular thickness (10–20 cm) layer of charcoal-rich, 416
 black fine silt. This organic-rich, black layer, contains 417
 magnetic Fe-rich microspherules and tektites at a 418
 depth of 1.70 m, reaching a peak concentration of 419
 260 microspherules (msph) per kg. An AMS ^{14}C date 420
 for this black mat layer (González et al. 2014) is 421
 $10,800 \pm 50$ BP ^{14}C BP. The lake sequence was then 422
 eroded by a lahar channel which was filled with lahar 423
 deposits composed of reworked Upper Toluca Pumice 424
 ash. This ash is $\sim 10,500$ ^{14}C BP and it is associated 425
 with the Nevado de Toluca Volcano activity (Arce 426
 et al. 2003; González and Huddart 2007). Two 427
 mammoths in the lahar sequence were radiocarbon 428
 dated to $11,100 \pm 80$ ^{14}C BP and $11,255 \pm 75$ ^{14}C 429
 BP. The calibrated age range of the mammoth bones is 430
 13,154–12,820 cal BP which overlaps the youngest 431
 part of the age range of the 12,835–12,735 cal BP for 432
 the YDP impact event (Kennett et al. 2015). The age of 433
 the mammoths may be coeval with the YDB event, but 434
 quite possibly it is older because the stratigraphy of the 435
 site. Finally, the sequence is capped by more lake 436
 sediments and an in situ rhyolitic ash dated to 437
 $10,016 \pm 39$ ^{14}C BP (Table 1). 438

439 Diatoms (Fig. 4) were studied from the same depths
 440 as the microspherules. A complete set of diatom
 441 abundance diagrams can be found in González et al.
 442 (2014). Epiphytic diatoms like *Navicula* sp., *Gom-*
 443 *phonema* sp. and *Pinnularia* sp. are found in the lower
 444 part of the section. Towards the top the assemblage
 445 changes to the motile benthic *Anomoeoneis*

Editor Proof

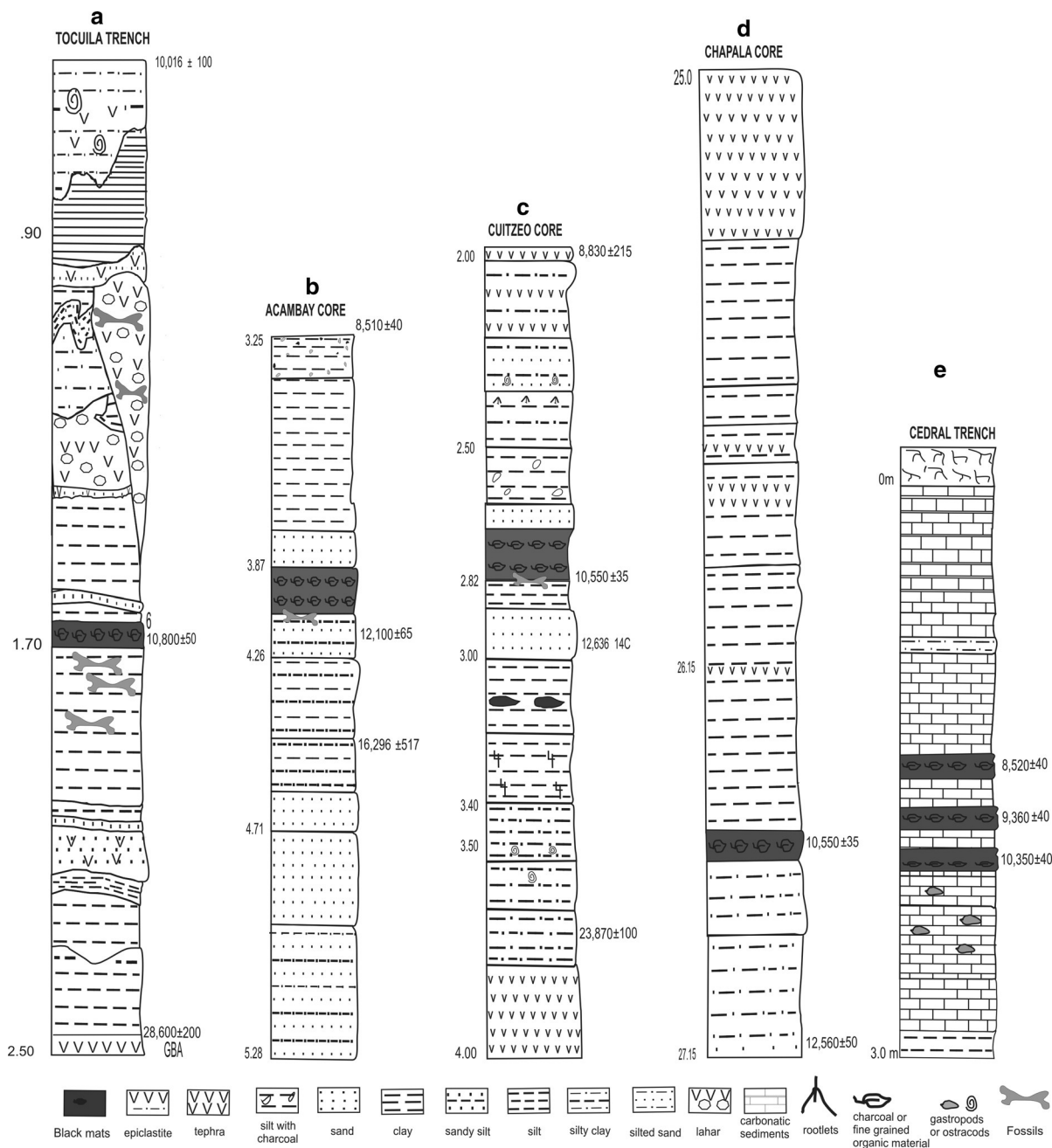


Fig. 2 Stratigraphy and AMS radiocarbon dates (uncalibrated) of the studied sites: **a** Tocuila trench, **b** Lake Acambay core, **c** Lake Cuitzeo core; **d** Lake Chapala core and **e** El Cedral trench. Black mats were present at all the sites

446 *sphaerophora*, *Surirella wetzelii*, and *Campylodiscus*
 447 (the last in small percentages). This association is
 448 replaced by *Surirella wetzelii* and *Anomoeoneis*
 449 *sphaerophora*. Sample 6 is from the black mat layer
 450 and is characterized by *Navicula* sp., *Gomphonema*

sp., and other motile benthic taxa, like *Anomoeoneis* 451
sphaerophora. 452

Pollen was analysed at Tocuila (González et al. 453
 2014), beginning with the Great Basaltic Ash at the 454
 base of the sequence which shows the presence of 455

456 *Pinus*, *Quercus* and *Alnus*. These taxa are in the same
 457 proportion as taxa of Asteraceae and Poaceae.
 458 Towards the top *Pinus* species dominate and in the
 459 black mat, silty organic-rich layer, that was laid down
 460 during the YD interval (see Table 1) there was an
 461 increase in the proportion of *Alnus*.

462 In this black mat layer, there is also a peak
 463 concentration of 260 Fe-rich microspherules (msph)
 464 per kg (see Tables 2, 3).

465 *Recently drained Lake Acambay*

466 This site is located in the central portion of the TMVB
 467 within the Morelia-Acambay and Tixmadeje E-W
 468 fault system (Suter et al. 1992, 2001). It forms part of
 469 the northern portion of the Acambay Graben, in which
 470 an extensive lake developed during the Last Glacial
 471 Maximum (LGM). A sediment core was taken at this
 472 site and the stratigraphy is described as follows
 473 (Fig. 2b):

474 Interval from 5.28 to 3.95 m depth: This interval
 475 has alternating layers of sand and sandy silt becoming
 476 silty towards the top of this layer (4.55 m). The silt
 477 was dated to $16,296 \pm 517$ ¹⁴C BP (see Table 1). The

contact with the upper layer is erosional, with a silty
 sand and associated with a mammoth mandible and a
 mastodont molar. Both are currently in the local
 Acambay Museum. A date at the top of the layer
 associated with the fossils (at 4.0 m depth) gave an
 uncalibrated date of $12,100 \pm 65$ ¹⁴C BP (Table 1).

An abrupt sediment change is observed from 3.95
 to 3.85 m depth, where there is an interval of peaty,
 carbon-rich, laminated black clay (black mat) which is
 located between two dates: $12,100 \pm 65$ and
 8510 ± 40 BP ¹⁴C BP (see Table 1). Above the black
 mat, the interval from 3.87 to 3.25 m became lami-
 nated, with silty clay toward the top.

Diatoms

In the interval from 5.28 to 4.20 m depth, high
 percentages (>70% of the total abundance) of the
 diatoms, *Stephanodiscus niagarae* and *Aulacoseira*
distans were present (Fig. 4b). From 4.20 to 3.95 m
 depth, *Aulacoseira distans* and *Fragilaria capucina*
 become the dominant taxa. The presence of this
 assemblage and the disappearance of *Stephanodiscus*
niagarae are the result of a lower lake level and

Table 2 Chemical composition of selected microspherules in four studied Mexican sites

Site	Weight percent													
	Spherule	C	O	Fe	Al	Si	Ca	Mn	Mg	S	K	Na	Ti	Mo
Lake Acambay	1	14.86	26.66	56.87	0.40	0.63	0.20	0.37						
	2	3.90	35.28	38.94										
	3	4.49	34.85	37.70	0.54	0.12								
	4	3.63	34.98	36.34										
	5	3.40	31.56	38.97	0.11	0.24								
Tocuila	6	35.5	42.12	22.34										
	7	19.83	50.96	1.64	4.99	16.07	2.02		1.05		0.71	2.07	0.27	0.40
	8	7.57	24.56	67.86										
	9		21.63	29.95		1.21	0.65			19.75				
	10	7.57	24.56	67.86										
Lake Cuitzeo	11	7.58	59.63	1.36		20.80	0.64		0.86	2.39	0.44	0.81		
	12	4.45	21.21	63.31										
	13	9.05	87.18	3.75										
	14		92.90	1.03	0.76	4.50	0.20					0.57		
	15	4.45	21.21	66.31										
Lake Chapala	16	3.04	31.56	38.97	0.11	0.24								
	17	3.63	23.48	61.53		1.43								

Acambay site contains nearly 100% iron oxide, with some C and minor amounts of trace elements in some spherules (Al, Si, Ca, and Mn), which are most likely surface contamination

Editor Proof

Table 3 Abundance of microspherules in black mats at different depths in the studied sites: Chapala, Cuitzeo, Acambay and Tocuila

	Chapala			Cuitzeo			Acambay			Tocuila		
	cm	Thick	Msph									
				45	10	120						
				25	10	125						
				15	5	80						
Above the event	40	20	Nd	10	5	310	20	10	Nd			
Maximum abundance	20	20	Nd	5	5	215	10	10	200	10	10	86
Below the event	0	20	394	0	7	2055	0	10	200	0	10	260
	-20	20	153	-10	10	220	-10	10	0	-10	10	0
	-40			-20	10	0	-20	10	0	-20	10	0
				-30	10	0				-10	10	0
				-40	10	0						
				-80	20	-						

Msph microspherule, *Nd* not determined

500 increased turbidity. From 3.95 to 3.85 m, diatoms
501 disappear almost completely from the sedimentary
502 record, and this layer becomes an organic-rich black
503 mat.

504 On top of this layer from 3.85 to 3.25 m, diatoms
505 reappear in the record with the presence of *Fragilaria*
506 species and in small percentages, *Epithemia turgida*
507 and *Eunotia minor*.

508 Pollen was not well preserved in the sampled
509 interval.

510 In the organic-rich black mat layer, magnetic Fe-
511 rich microspherules were found, reaching a peak
512 abundance of 200 msph per kilo at a depth of 3.90 m
513 below the surface (Tables 2, 3), and they display a
514 wide variety of forms, including ovoid shapes, and
515 reach sizes of up to 60 μm .

516 *Lake Cuitzeo*

517 For Israde-Alcántara et al. (2012), obtaining accurate
518 dates for this lake's strata was difficult because of
519 significant injections of older carbon of unknown
520 origin into the lake basin. Kinzie et al. (2014) used a
521 new date of $12,897 \pm 187$ cal yr BP from a nearby
522 trench to produce a new age-depth model identifying
523 the YD onset, and this new model supports the
524 conclusion of Israde-Alcántara et al. (2012) that the
525 depth corresponding to the YD onset was correctly
526 identified, based that conclusion on independent
527 palynological and climatic studies of Lake Petén Itzá

in Guatemala, La Chonta Bog in Costa Rica, Lake La
Yeguada in Panama, and the Cariaco Basin in the
Caribbean (Bush et al. 2009; Islebe and Hooghiemstra
2006; Mahaney et al. 2010a, b). Those studies showed
that there is only one stratigraphic interval at each site
that displays extraordinary climatic, environmental,
and biotic changes, and in each case, this interval
occurs at or near the age of the YD onset.

The description of the stratigraphy and the paleo-
environments of a core taken from the depocenter of
Lake Cuitzeo has been described in Israde-Alcántara
et al. (2012). Here we discuss the interval from 4.0 to
2.0 m depth (Fig. 2c) as follows: Overlain by a 22 cm
epiclastite layer (reworked volcanic sediment), a dark
green clayey silt is present from 3.78 to 3.40 m in
depth, becoming laminated toward the top and
containing abundant gastropod remains. From 3.40
to 3.03 m, the strata comprise finely laminated black
clay, overlain by a 17 cm silty clay. Transitionally
from 3.00 to 2.90 m in depth, the silty clay changes to
dark, very fine sand with feldspar, halloysite, and
montmorillonite clasts. From 2.90 to 2.85 m in depth,
there is a plastic, dark brown clay with abundant
organic matter and beige-colored, millimeter-sized
clay clasts, with white veins. Above this stratum, there
is a texturally mature fine sand, composed mainly of
albite and mica.

From 2.85 to 2.75 m in depth, macro-charcoal
fragments become much more abundant (Fig. 3). At
2.65 m, the number of macro-charcoal particles

572 maintain low concentrations, reaching maximum
573 values at 2.90 m in depth with 5×10^5 grains/g
574 sediment, and pollen indicates a tendency towards a
575 deeper lake.

576 Transitionally the interval from 3.00 to 2.85 m
577 depth, shows abundant sponge spicules and the
578 frequency of *Staurosira* decreases. From 3.0 to
579 2.80 m pollen of both arboreal and non-arboreal
580 species markedly decrease toward the top and almost
581 disappears from the basin in this interval. From 2.85 to
582 2.75 m depth *Stephanodiscus niagarae* forms an
583 almost monospecific community, amounting to
584 $\sim 85\%$ of the total diatom taxa, in only one sample.
585 At 2.80 m in depth and all periphytic and saline
586 diatom taxa disappear. Immediately after the *Stephan-*
587 *odiscus niagarae* bloom, macro-charcoal fragments
588 become much more abundant, amounting to up to
589 1×10^5 macrocharcoal particles per gram of sediment
590 (Fig. 3). Microspherules in the 2.82–2.75 m depth
591 interval, show a peak abundance at 2055 msphs per
592 kg.

593 The interval from 2.70 to 2.50 m in depth is
594 composed of massive black clay with interlayered
595 gray fine sand in which the planktonic diatom
596 *Stephanodiscus niagarae* disappears, at the the same
597 time as *Staurosira construens*, a periphytic to plank-
598 tonic diatom, and other epiphytic taxa become dom-
599 inant again. The presence of turbid conditions at that
600 depth is indicated by the diatom *Aulacoseira granu-*
601 *lata*, *Staurosira construens* increases in abundance
602 after the black mat strata, but does not reach percent-
603 ages indicative of the previous warm conditions.
604 *Typha* pollen (Fig. 3) increases to its maximum, and
605 arboreal and non-arboreal taxa indicates evidence for
606 an increase in forest disturbance in the basin sur-
607 rounding the lake (Israde-Alcántara et al. 2010). In the
608 interval between 2.50 and 2.00 m *Stephanocyclus*
609 *meneghiniana* and other saline diatom taxa appear in
610 the early Holocene.

611 Lake Chapala

612 Zárata del Valle et al. (2014) drilled a 27.15 m long
613 core in the depocenter of Lake Chapala, the largest of
614 the lakes in the TMVB. From ca. 27.15 to 26.60 m the
615 core consists of a homogeneous, dark gray, silty clay.
616 At 27.13–27.00 m appears a silty organic horizon that
617 was radiocarbon dated to $12,560 \pm 50$ ^{14}C BP (CHD-

Ba6). Towards the top the silt become more organic 618
(26.60–26.45 m), reaching TOC values of up to 3%. 619

620 A tephra layer in transitional contact was observed
621 towards the top at the interval 26.16–26.15 m in depth.
622 From 26.15 to 25.00 m., there are sub-laminae of gray,
623 clayey silts that are capped by volcanic, silty sands.
624 Other tephra layer appear at 25.70 m.

625 At the base of the core (Figs. 2d, 4) from the
626 depocenter of Lake Chapala diatoms from the Pleis-
627 tocene–Holocene boundary at 26.60 m, are character-
628 ized by *Stephanodiscus niagarae* reaching 95% of the
629 total of taxa indicating high lacustrine levels and low
630 salinity just before the YD. This episode is followed by
631 a decrease of lake level and enhanced turbidity
632 documented by *Aulacoseira granulata* with percent-
633 ages $>80\%$.

634 Pollen from the Pleistocene–Holocene transition
635 shows that *Pinus* is dominant and is followed by
636 *Quercus*, *Asteraceae* and *Poaceae*.

637 In the interval from 26.60 to 26.45 m, magnetic Fe-
638 rich microspherules reach a peak abundance of
639 394 msphs per kg, ranging in size between 60 and
640 80 μm . They are composed mainly of Fe and Si,
641 although some also contain Al (see Tables 2, 3).

642 El Cedral

643 The El Cedral site is located in the Mesa Central of
644 Mexico in the northern state of San Luis Potosí and is
645 surrounded by Cretaceous carbonate rocks of the
646 Sierra Madre Oriental. Intra-basins that formed in the
647 Monterrey thrust fault allowed the development of
648 ponds fed by hydrothermal activity for several thou-
649 sand years. These ponds were an important refuge for
650 vertebrates, including megafauna (e.g. mammoths,
651 horses). The presence of Paleoindians during the Last
652 Glacial Maximum (LGM) was suggested by proposed
653 hearths dated at $31,850 \pm 1600$ ^{14}C BP (I-10483)
654 (Lorenzo and Mirambell 1986; Mirambell 2012). The
655 stratigraphy at El Cedral (Fig. 2e) consists of a 3-m-
656 thick gray-white calcrete at the top, interlayered with
657 silty carbonate muds (Fig. 5). In the central part of the
658 sequence, three 8–10 cm thick, black charcoal- and
659 soot-rich layers interrupt the homogeneous calcareous
660 sequence (Fig. 5). The oldest black level dates to
661 $10,350 \pm 40$ ^{14}C BP, and so, was deposited during the
662 YD.



Fig. 5 El Cedral springs site (San Luis Potosi) showing the three black mat organic layers. See Fig. 2e and Table 1 for the stratigraphy and radiocarbon dates obtained for the site

663 There are no diatoms in the deposits but there are
664 ostracods (*Darwinila* sp.) that appear in the light-
665 yellow silty carbonate mud levels.

666 Fewer than 50 pollen grains were found in the
667 samples analyzed. The few pollen grains in the
668 samples belong to aquatic taxa, such as *Cyperus*,
669 *Typha*, *Potamogeton*, and *Chenoamaranthaceae*. Ter-
670 restrial pollen grains belonging to Poaceae, Aster-
671 aceae, *Quercus*, and *Pinus* were also observed.

672 Results from the EDS analyses of the carbonate
673 fraction of the white deposits show that they contain
674 35.79% Ca and minor amounts of Si, Na, Fe, and Mn.
675 In the black soot deposits, the dominant element is Si
676 and C is followed by Ca, Na, Al and Fe.

677 The three black mats from El Cedral lack Fe
678 microspherules. The oldest is YD in age and the
679 younger two are Holocene in age.

Scanning electron microscopy (SEM) 680

In Tocuila, Lake Acambay, Lake Cuitzeo and Lake 681
Chapala, Si-rich and Fe-rich microspherules occurred 682
at the YDB levels (see Fig. 6; Tables 2, 3), but none at 683
the El Cedral site. The majority of the microspherules 684
were rounded and their structures varied from nearly 685
smooth, dendritic, polygonal, cob-like, to complex 686
filigree (Fig. 6a–d), and had diameters ranging from 8 687
to 130 μm . In some cases, the microspherules dis- 688
played a hollow, shell-like morphology that allowed 689
observations of the interior of the microspherules 690
(Fig. 6b). One microspherule showed a flattened 691
bottom, surrounded by a skirt with multiple compres- 692
sion rings, indicating the molten microspherule under- 693
went significant deformation during a high-velocity 694
collision with another particle (6d) (see a similar 695
spherule in Fig. 5d in Israde-Alcántara et al. 2012). 696
Results of the EDS elemental spectrum for each 697
microspherule, indicate that Fe and O are the dominant 698
elements in the compositions of most spherules, with 699
formation temperatures of >1450 $^{\circ}\text{C}$, while several 700
were dominated by Si, with minor abundances of Al, 701
Mg, Ca, Mn, S, K, Na, Ti, and Mo (Table 2). Pieces of 702
meltglass (tektites) were also observed (Fig. 6.b.6), 703
composed mostly of Fe, Si, and Al and with diameters 704
up to about 400 μm . 705

Discussion 706

Lake sedimentation and paleoenvironments 707

At Tocuila the basal tephra correlates to the Great 708
Basaltic Ash (GBA $28,600 \pm 200$ ^{14}C BP). The 709
sediments contained diatoms and pollen that indicated 710
that the ash fell into a shallow lake with a macrophyte 711
border in a landscape of open temperate forest. 712

Then there was an increase in the lake level with 713
high electrolyte content as suggested by the presence 714
of *Surirella wetzelii*, *Campilodiscus clypeous* and 715
other saline taxa. 716

Towards the top of the sequence, the lake continued 717
to have a high electrolyte concentration with *Surirella* 718
wetzelli and *Anomoeoneis sphaerophora*. In this 719
episode there was an increase in *Pinnularia* sp., and 720
Navicula sp. suggesting the establishment of aquatic 721
macrophytes along the lake margin. Arboreal forest 722

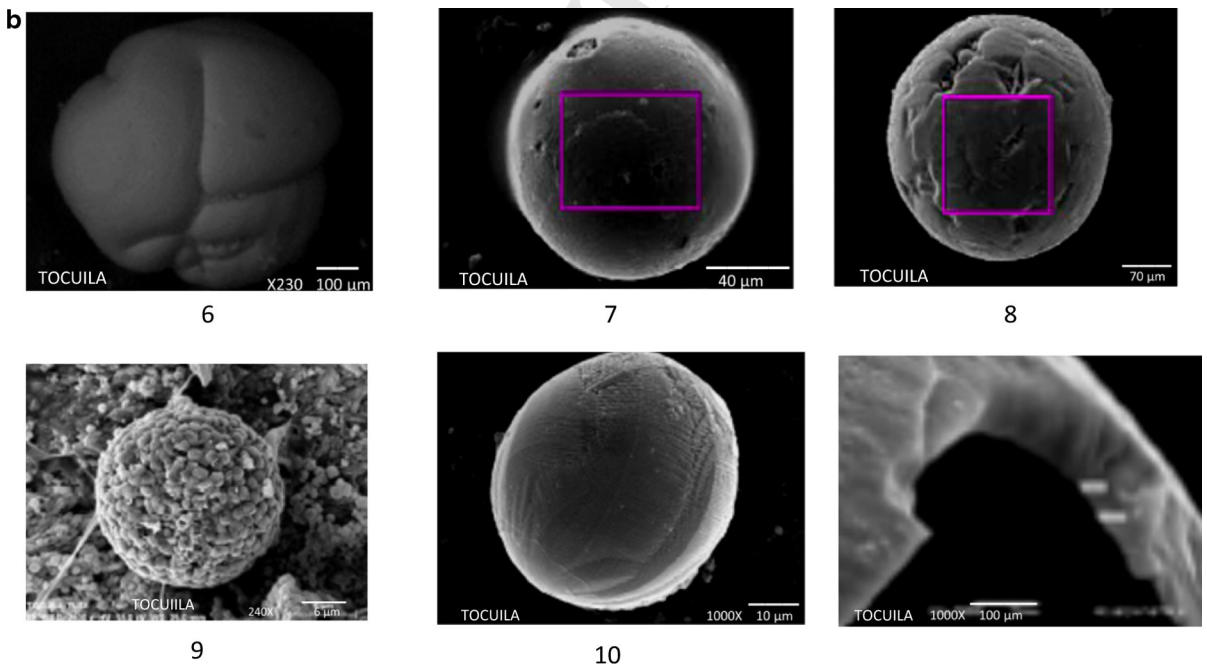
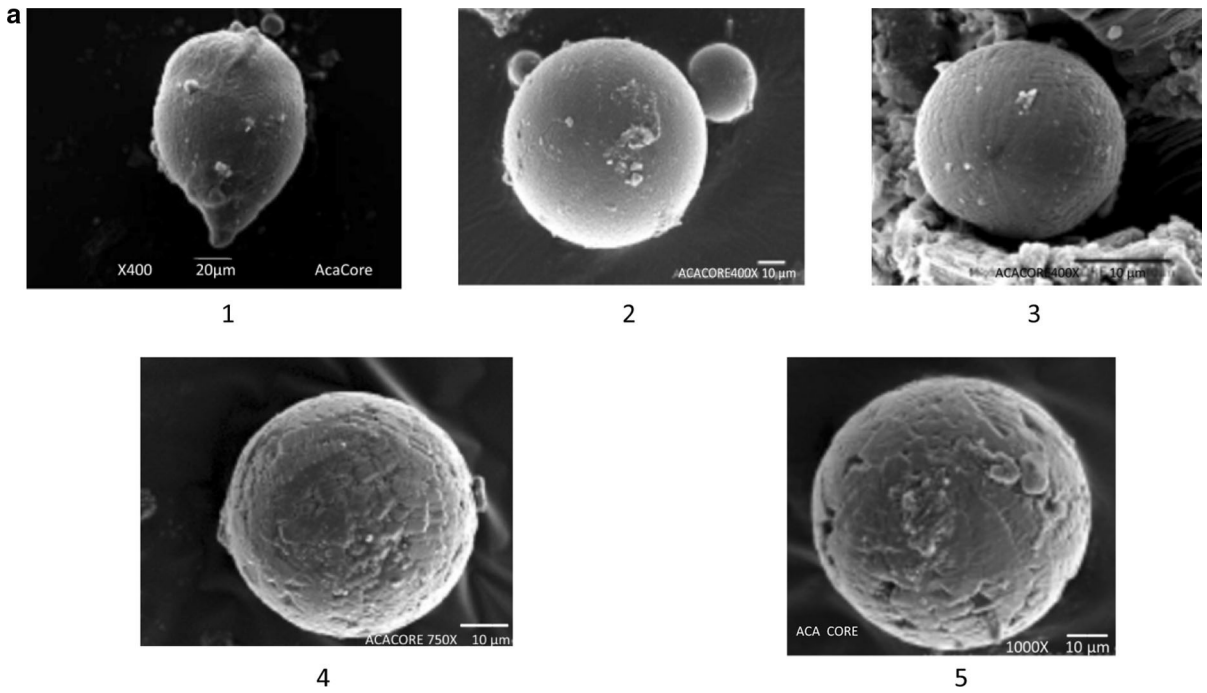
Fig. 6 Selected SEM images of magnetic microspherules from the Mexican sites, found in organic-rich layers, showing their distinctive surface structure. All microspherules display distinctive patterns, indicative of high-temperature melting and quenching. C was used to coat the samples. **a** Acambay core; **b** Tocuila trench; **c** Cuitzeo core; **d** Chapala core. **a.1** Acambay core—110- μm -long, aerodynamically shaped, teardrop-like microspherule displaying dendritic surface structure. Contains $\sim 85\%$ Fe and O with minor amounts of trace elements, Al, Si, Ca, and Mn, which are most likely surface contamination. Several rounded to sub-rounded objects are visible on the surface and appear to have been incorporated into the parent object while in a molten state. Composition also shows $\sim 15\%$ C, which most likely represents SEM coating material. **a.2** Acambay core—round, 80- μm -wide microspherule displays almost perfectly formed dendritic texture. Composition is nearly 100% iron oxide, indicating formation temperatures of 1450 $^{\circ}\text{C}$. The high iron content and formation temperature preclude an origin by volcanism, which typically produces volcanic glass spherules. Two smaller, independent spherules are around the larger one. **a.3** Acambay core—20- μm -wide microspherule showing dendritic surface. Contains $\sim 73\%$ Fe and O with minor amounts of Al, Si, and C, the latter probably representing SEM coating material. Shows dendritic structure in which lines of crystallization radiate away from a point at lower left of center, from which the molten particle first began to crystallize. **a.4** Acambay core—70- μm -wide spherule with large polygonal plates, indicating that this spherule stayed molten slightly longer than spherules with finer textures, giving the crystals more time to grow. The spherule is nearly 100% Fe and O, indicating formation temperatures of >1450 $^{\circ}\text{C}$. The small amount of C is likely from the SEM coating. **a.5** Acambay core—another 70- μm -wide spherule with polygonal plates. As the plates crystallized, they met and stopped growing, leaving small gaps between some of the plates. Composition is nearly 100% Fe and O, with minor amounts of other elements. **b** Un-numbered, Tocuila trench—part of a 130- μm -wide, hollow, broken microspherule with well-developed dendritic internal structure displayed on the ~ 7 μm -thick cross-section of the shell. Hollow morphology is the typical result of rapid melting of Fe-rich parent materials, in which volatiles become trapped inside the spherule. Composition is nearly 100% Fe and O. **b.6** Tocuila trench—390- μm -wide piece of meltglass (tektite) showing creases between multiple lobes that appear to have been fused together while molten. Composition is a mixture of 64% Fe and O with 36% C; the latter value is too high, to be the result from the SEM coating. This object formed from rapidly mixing and quenching of C and molten Fe oxide at temperatures >1450 $^{\circ}\text{C}$. **b.7** Tocuila trench—60- μm -wide aluminosilicate microspherule, showing fine-grained dendritic surface, due to higher Si content. Composition is a complex mix of 16% Si, 5% Al, 2% Ca, 2% Na, 1% Mg, 51% O, 20% C, and minor amounts of other elements. The spherule is pitted either because it is hollow or because of degassing when molten. **b.8** Tocuila trench—100- μm -wide microspherule showing large, polygonal plates with occasional gaps where plates failed to intersect at boundaries. Composition is nearly 100% Fe and O, with some C from SEM coating. **b.9** Tocuila trench—25- μm -wide, non-impact-related framboid, commonly found at many YDB sites. Composition is 20% S, mixed with 30% Fe and 22% O, similar to pyrite, with small amounts of contaminants. Object formed over time authigenically, rather than rapidly like YDB spherules. **b.10** Tocuila trench— ~ 50 - μm -wide microspherule displaying a quenched structure. Spherule shows lines of crystallization radiating away from a point at the lower left, which was the point at which the molten particle first began to crystallize. Spherule in **a.3** above displays the same morphology. Composition is nearly 100% Fe and O, with 8% C from SEM coating. **c.11** Cuitzeo core—8- μm -wide silicate spherule with distinctive patterned surface. With high Si content of 20% with 60% O, 1% Fe, and minor amounts of impurities. **c.12** Cuitzeo core—100- μm -wide microspherule showing a dendritic surface. Composition is nearly 100% Fe and O. **c.13** Cuitzeo core -semi-rounded, non-impact-related titanium-iron oxide (ilmenite) grain, showing eroded edges and planar surfaces without ornamentation. This is a typical, unmelted grain that is morphologically different than high-temperature, melted spherules. **c.14** Cuitzeo core -unidentified, unmelted, patterned piece of detrital material. Texture suggests possible cracking by desiccation or by brief exposure to very high temperatures. **c.15** Cuitzeo core—130- μm -wide microspherule, showing distinctive polygonal structure, composed of crystalline plates that stayed molten for relatively longer than other spherules at these sites. **d.16** Chapala core—100- μm -wide spherule with polygonal plates. Composition is nearly 100% Fe and O, with small amounts of contamination by Al and Si. **d.17** Chapala core—65- μm -wide microspherule displaying evidence of deformation which suggests high-velocity collision with another particle. Collision was energetic enough to form multiple compression rings around the lip of the bottom surface, along with distinctive striations that lead away from the collision towards the opposite end of the spherule. Composition is nearly 100% Fe and O, with small amounts of Si and C

723 taxa was recorded around the lake. This was associated
724 with a wetter environment dominated by *Pinus*.

725 At $10,800 \pm 50$ ^{14}C BP an environmental change
726 indicating a dilution episode is suggested by the
727 increase of several epiphytic taxa dominated by
728 *Navicula* sp., *Gomphonema* sp., the *Fragilaria* group,
729 *Achnanthes* sp. and *Eunotia* sp. (the latter in a small
730 percentage). This floristic composition indicate that
731 the margins of Lake Texcoco had a freshwater marshy
732 environment with cooler conditions (Bradbury 1971)
733 as suggested by an increase in the proportion of the
734 temperate forest tree *Alnus*. In this layer of YD age,

735 there is also a peak concentration of 260 Fe-rich
736 microspherules (msph) per kg (see Table 3). Above
737 this layer, pollen and diatoms are not well preserved
738 and are mixed with rhyolitic ash that fell into a shallow
739 lake.

740 In Lake Acambay the high percentages of planktonic
741 taxa dominated by *Stephanodiscus niagarae* and
742 *Aulacoseira distans*, followed by *Aulacoseira granu-*
743 *lata* and the planktonic *Fragilaria capucina* indicates
744 that prior to the YD there was a deep but fluctuating,
745 turbid lake. In the YDB black mat layer there are no
746 diatoms. After the YDB, diatoms colonize again with



Editor Proof

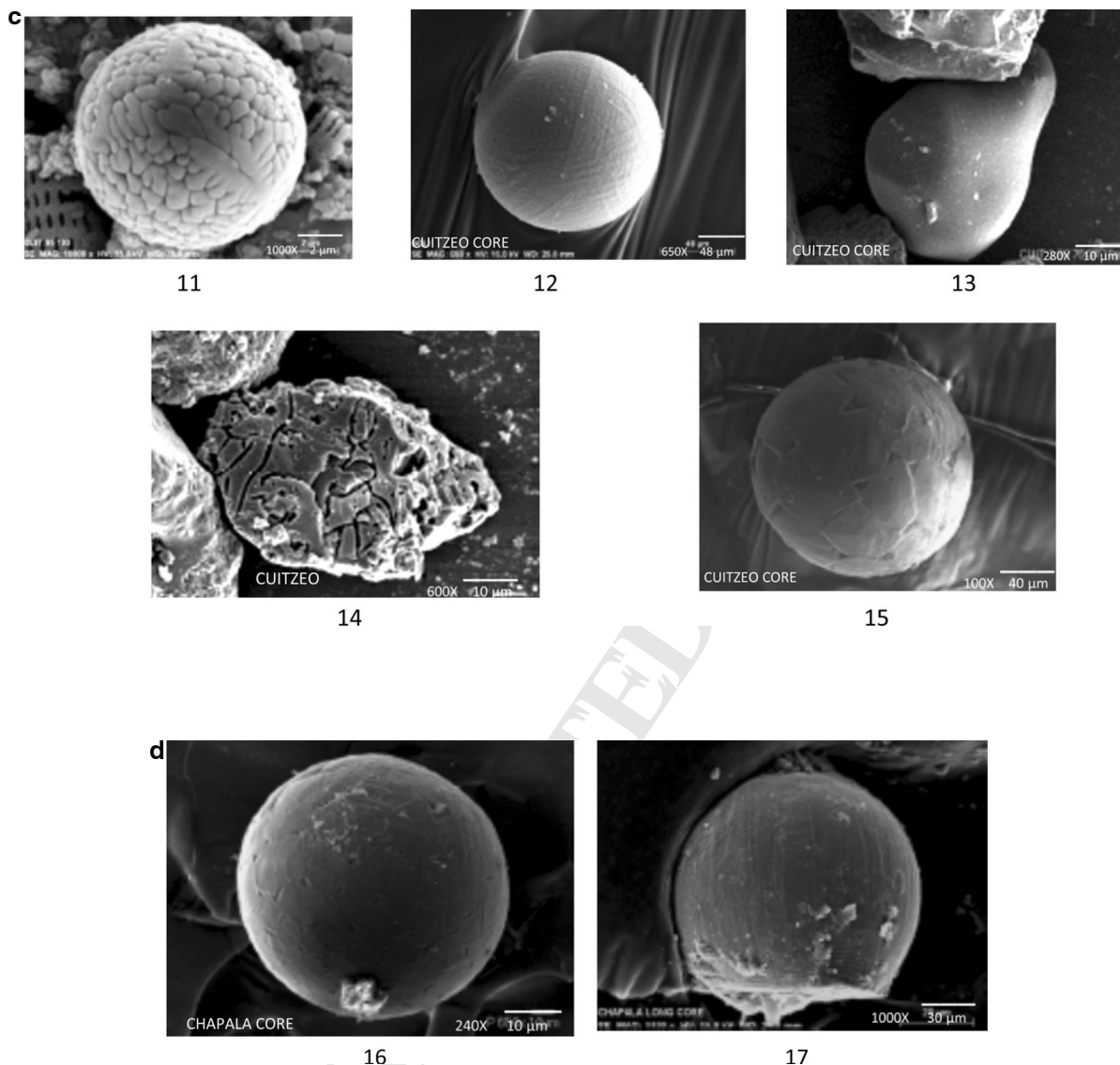


Fig. 6 continued

747 the presence of *Fragilaria* species and in small
 748 percentages (less than 5%), *Epithemia turgida* and
 749 *Eunotia minor*, which indicate a slightly acid marsh.
 750 Pollen was not well preserved in the YD sampled
 751 interval.

752 In this organic-rich black mat layer, magnetic Fe-
 753 rich microspherules were found, reaching a peak
 754 abundance of 200 msph per kilo at a depth of 3.90 m
 755 below the surface, and they display a wide variety of
 756 forms, including ovoid shapes, and reach sizes of up to
 757 60 μm (Fig. 6a).

In Lake Cuitzeo, during the pre-YD the diatom
 communities indicate a shallow lake dominated by
Fragilaria species and aquatic taxa maintained low
 concentrations. There were low concentrations of
 arboreal pollen (*Pinus*, *Quercus* and *Alnus*) from
 around the lake.

The transition to YD in Lake Cuitzeo is noted at
 2.85 m and dated to 12,870 years cal yr BP. This
 occurred in a 7–10 cm thick black mat layer, in which
 it was noted a rapid deepening of the lake indicated by
 the diatom *Stephanodiscus niagarae* in only one

758
 759
 760
 761
 762
 763
 764
 765
 766
 767
 768

769 interval (Fig. 3) and *Botryococcus* (Israde-Alcántara
770 et al. 2012). Abundance drastically decreases after the
771 event, possibly related to fires that occurred during the
772 event. At 2.85–2.80 both arboreal and non-arboreal
773 species markedly decrease and in the lake mainly
774 *Typha* remains. At 2.80–2.70 m depth, there is a
775 massive black silty clay with macro-charcoal. The
776 abundance of charcoal suggests widespread fires at the
777 YD boundary around Lake Cuitzeo. At 2.85–2.75 m
778 depth, there is a peak abundance of microspherules at
779 2055 msphs per kg (Table 3; Fig. 6c).

780 At Lake Chapala diatoms from the Pleistocene–
781 Holocene transition (Fig. 4), as at Lake Cuitzeo,
782 record a dominance of *Stephanodiscus niagarae*,
783 reaching 95% of the total taxa which indicates high
784 lake levels. This episode is followed by a decrease in
785 lake level and enhanced turbidity documented by
786 *Aulacoseira granulata* at over 80%. Magnetic Fe-rich
787 microspherules with low Al were observed in the
788 interval from 26.60 to 26.45 m, reaching a peak
789 abundance of 394 msphs per kg, with diameters
790 between 60 and 80 μm (Table 3; Fig. 6d).

791 At the El Cedral site, the oldest black mat level,
792 dates to $10,350 \pm 40$ ^{14}C BP, so it's YD in age
793 (Fig. 2e). The presence of ostracods such as *Darwin-*
794 *ula* sp., in the light-yellow colored levels indicate a
795 shallow lake benthos and could be indicative of pools
796 with hydrothermal activity, at temperatures between
797 10 and 30 $^{\circ}\text{C}$, with neutral pH and dissolved oxygen
798 ca. 14 mg/L (Ruiz et al. 2013).

799 In several cores taken from the studied lake
800 sediments, a distinctive interval interpreted as a black
801 mat was found, in which major sharp environmental
802 changes are identified. In every case, except at the El
803 Cedral site, magnetic microspherules were found
804 associated with this interval, which radiocarbon dates
805 identified as being at, or near, in age to the onset of the
806 YD.

807 Black mats

808 In this study, we have identified distinctive black
809 mat horizons at these Mexican sites. The black mats
810 date at, or near, the YD onset at three of the studied
811 sites: Lakes Texcoco (Tocuila), Cuitzeo and Cha-
812 pala. A fourth site, Lake Acambay, had insufficient
813 dating control, and it can only be said that the black
814 organic-rich layer is late Pleistocene or early

Holocene in age. These sites are located in lacustrine
815 environments (Cuitzeo, Acambay, and Chapala
816 in central western Mexico) and lake nearshore
817 (Tocuila, in the Basin of Mexico), but they all
818 share similar proxy signatures.
819

820 Black mats at four of the sites (Cuitzeo, Acam-
821 bay, Chapala, and Tocuila) display evidence of a
822 cosmic impact event, indicated by high-temperature,
823 melted microspherules within the black mat layer.
824 The microspherules, charcoal and soot are consistent
825 with the hypothesis that the YDB impact event
826 caused sudden wildfires that consumed the local
827 biomass, as in other YDB sites in seven countries
828 across three continents (LeCompte et al. 2012;
829 Mahaney et al. 2014; Wittke et al. 2013). The depth
830 to the YDB layer in the studied lakes varies widely,
831 because the local sedimentation rates vary, with the
832 YD at 2.80, 3.87 and 1.90 m at Cuitzeo, Acambay
833 and Tocuila respectively.

834 In some sections there was a sharp unconformity,
835 as observed in Lake Cuitzeo and Lake Chapala
836 (Figs. 2c, d, 3). In the largest lakes (Chapala and
837 Cuitzeo) there was an increase in water depth and
838 turbidity during the Pleistocene–Holocene transition.
839 In the border of Lake Texcoco, at Tocuila, there was
840 a change from more saline conditions to fresh water
841 at the YD onset.

842 In Lake Acambay there needs to be further dating
843 control to establish the age of the sequence, especially
844 at the YD interval.

845 At the El Cedral springs site, there are three
846 different black mat horizons, each resulting from
847 marshy environments, as indicated by algae and other
848 aquatic herbs and pollen grains of *Typha*, *Cyperus*,
849 *Potamogeton* and Chenopodiaceae. The oldest
850 black mat at the site was dated at $10,350 \pm 40$ ^{14}C BP,
851 which is YD in age but it was not dated at the base of
852 the deposit. The three black mats lack microspherules
853 but have evidence of burning. The two younger black
854 mats are Holocene in age and indicate that not all black
855 mat origins are related to impact events (Quade et al.
856 1998).

857 The results from this study suggest that the YD
858 climate initiated with a short period of increased
859 precipitation which is comparable with other regional
860 and hemispheric records across the world. In central
861 Mexico after the YD the lakes were characterized by
862 low lake levels (Ortega-Guerrero et al. 2010).

863 Magnetic microspherules

864 Spherules concentration varies from lake to lake (see
865 Table 3) and we suggest this is associated with the
866 distance to impact, conditions of deposition and post-
867 depositional environments, including later weather-
868 ing. At Lake Cuitzeo the largest concentration of Fe
869 micro-spherules was found. For this reason, this site
870 has been studied and dated more intensively (Israde-
871 Alcántara et al. 2012).

872 In Table 3 we report the abundance of micro-
873 spherules found in four Mexican lakes. In Chapala at
874 20 cm below the enriched level a total of 153
875 spherules per kg were counted; towards the top none
876 was detected. In Cuitzeo we report at total of
877 2055 spherules per kg. This is the lake with the largest
878 microspherule abundance. In the upper levels of the
879 core the spherules are up to 45 cm above the black mat
880 deposit, interpreted here as reworking in this highly
881 tectonic lake.

882 In Lake Acambay the same number of micro-
883 spherules were found at the base and center of the
884 black mat.

885 In Tocuila the highest abundance was at the middle
886 of the black mat with 260 spherules per kg and towards
887 the top of the black mat a total of 86 spherules per kg
888 were counted.

889 At the sites the shape of the spherules is often ovoid,
890 polygonal, dendritic or filigreed (Fig. 6a–d), with
891 textures produced by rapid melting and quenching
892 during the impact event (Petaev and Jacobsen 2004).
893 The spherules show a further range of morphologies,
894 including hollow shells (Fig. 6b), and a flattened side
895 with a “skirt” structure caused by a high-velocity
896 collision (Fig. 6d). Andronikov et al. (2016) discussed
897 some possible formation mechanisms for producing
898 hollow magnetic microspherules, such as by de-
899 gassing of volatile elements at high temperatures
900 ranging from ~1200 to ~2200 °C, the melting point
901 of quartz (Dressler and Reimond 2001).

902 Based on previous studies, the origin of the Fe-rich
903 magnetic microspherules was investigated. First, by
904 comparing those found in the sites to those formed
905 anthropogenically as modern industrial pollution par-
906 ticles (Israde-Alcántara et al. 2012; Wittke et al.
907 2013). Because the Fe-rich magnetic microspherules
908 found are associated with other proxies, such as
909 nanodiamonds (Lake Cuitzeo), and are deeply buried,
910 in some cases, at a depth of up to 14 meters, their depth

precludes an origin from recent anthropogenic activ- 911
ity. Next, magnetic spherules that are known to be 912
produced by volcanism were compared in Israde- 913
Alcántara et al. 2012. Volcanic spherules are com- 914
posed of volcanic glass that is dominated by high 915
concentrations of Si and Al, whereas the spherules 916
from the studied Mexican sites here are dominantly 917
enriched in Fe and O, an elemental composition that 918
does not occur in volcanic spherules (Bunch et al. 919
2012; Wittke et al. 2013). Also authigenesis was 920
considered as a source, but the dendritic surface 921
morphology of the spherules indicates rapid, high- 922
temperature melting and quenching, which precludes 923
authigenesis. Lastly, it was considered whether the 924
magnetic spherules might be cosmic in origin, but this 925
possibility can be ruled out by the geochemical 926
composition of the spherules, which contain very 927
low levels of Mg, a key component of cosmic material, 928
which typically contains more than 10% MgO. In 929
addition, one of the melted microspherules from the 930
sites contains titanium, which rarely occurs in cosmic 931
material (Bunch et al. 2012; Wittke et al. 2013). 932

933 Thus, the microspherules likely formed from a
934 cosmic impact event that melted rocks and surficial
935 sediments and soils. This possibility is confirmed by
936 comparing the geochemical composition of the micro-
937 spherules to those from known impact events, as
938 discussed in previous studies, including Bunch et al.
939 (2012), Wittke et al. (2013), and references therein. 939

940 **Conclusions**

941 An anomalous black sediment layer, produced during
942 the YD interval, was recognized in three different lake
943 sites from central Mexico (Lakes Acambay, Cuitzeo
944 and Chapala) and also in a nearshore lake environment
945 at Tocuila, close to a former shoreline of Lake
946 Texcoco in the Basin of Mexico. These black mat
947 layers contain large amounts of organic material,
948 charcoal, soot, nanodiamonds (only studied at the
949 Cuitzeo site, Israde-Alcántara et al. 2012), magnetic
950 Fe-rich microspherules (some with aerodynamic
951 shapes and evidence of high-velocity collisions) are
952 a common feature in four of the five sites analysed.
953 These unusual materials were not observed above or
954 below the black mat sediments at these sites. Soot and
955 charcoal observed in the YD layers are evidence of
956 regional fire across areas separated by 1200 km and

957 are potentially associated with a cosmic impact event
958 of intercontinental dimensions, consistent with the
959 YDB impact hypothesis.

960 Paleoenvironmental reconstructions using pollen,
961 diatoms and geochemical proxies show that for the YD
962 there was major environmental change. These obser-
963 vations are consistent with reports at numerous other
964 YDB sites around the world, suggesting that this event
965 changed climatic patterns in the Northern Hemisphere,
966 as well as parts of the Southern Hemisphere. The
967 Mexican sites suggest that most of the environmental
968 changes resulted from the following:

- 969 (a) The proposed impactor changed local and
970 regional climate, producing an abrupt change
971 in the structure and composition of vegetation.
972 The lack of vegetation caused an increase in
973 runoff that result in major changes in
974 sedimentation.
- 975 (b) Widespread wildfires destroyed vegetation bio-
976 mass, creating large amounts of charcoal and it
977 is likely that more sediment moved downhill
978 during rainstorms.
- 979 (c) Increased precipitation and lake turbidity, pro-
980 duced a rise in lake levels, as indicated by the
981 presence of the diatoms *Stephanodiscus nia-*
982 *garae* and *Aulacoseira* spp.
- 983 (d) Environmental changes caused by the impactor
984 are likely to have contributed to major changes
985 in the megafaunal and human population and
986 distribution patterns, along with the associated
987 climate changes.
- 988 (e) The three black mats at El Cedral have no
989 microspherules. The older black mat is YD in
990 age but the obtained date is not from the base of
991 this layer. The other two black mats are
992 Holocene but they require more research to
993 determine their origin.
- 994 (f) For future work, it is necessary to obtain cores
995 and stratigraphic sections with higher resolution
996 and closer dating control in other areas in
997 Mexico in which the evidence of the YD impact
998 event could potentially be present.

999 **Acknowledgements** The authors wish to thank the economic
1000 support from CONACYT, Mexico, project CB266555-2015,
1001 and the Universidad Michoacana de San Nicolás de Hidalgo
1002 CIC 2015, 2016. Authors want to thank to Dr. Hong Chun Li,
1003 for the Acambay core dating, Dr. Pedro Zarate for sharing the C
1004 ¹⁴ dating and samples from the base of the Chapala long core,

Ricardo Saucedo, José Ramón Torres, of University of San Luis
Potosí for the help in field work at El Cedral and Francisco
Solorio and Lourdes Mondragón for the SEM analysis at the
Instituto de Investigaciones Metalúrgicas y Materiales and
Tecnológico de Morelia respectively and the helpful comments
of two referees and the editor that improved this manuscript.

References

- Almanza Alvarez JS, Israde I, Segura-García V (2016) Peri-
phytic diatoms of lake Patzcuaro, Michoacán, Mexico.
Hidrobiologica 26(2):161–185
- Andronikov AV, Lauretta DS, Andronikva IE, Maxwell RJ
(2011) On the possibility of a Late Pleistocene extrater-
restrial impact: LA-ICP-MS analysis of the Black Mat and
Usello Horizon samples. In: Abstract at 74th meteoritical
society meeting, London, UK, August 8–12
- Andronikov AV, Rudnickaite E, Dante S, Lauretta IE, Andro-
nikova K, Šinkunas P, Melešyte M (2013) In search for
fingerprints of an impact: HR-ICP-MS. Study of late
Pleistocene lake sediments of Lithuania. In: Conference:
Palaeolandscapes from Saalian to Weichselian, South
Eastern Lithuania. International field symposium
- Andronikov AV, Andronikova IE, Clayton W, Loehn W,
Lafuente B, Ballenger J, Crawford GT, Lauretta DS (2016)
Implications from chemical, structural and mineralogical
studies of magnetic microspherules from around the lower
Younger Dryas Boundary (New Mexico, USA). *Geogr Ann
Ser A Phys Geogr* 98(1):39–59
- Arce JL, Macias JL, Vazquez Selem L (2003) The 10.5 ka
Plinian eruption of Nevado de Toluca, Mexico, strati-
graphical and hazard implications. *Geol Soc Am Bull*
15:230–248
- Battarbee R, Jones V, Flower R, Cameron N, Bennion H, Car-
valho L, Juggins S (2001) Diatoms. In: Smol J, Birks J, Last
W, Bradley R, Alverson K (eds) Tracking environmental
change using lake sediments, vol 3. Terrestrial, algal, and
siliceous indicators. Springer, Berlin, pp 155–202
- Bradbury JP (1971) Paleolimnology of Lake Texcoco, Mexico,
evidence from diatoms. *Limnol Oceanogr* 16:180–200
- Bronk-Ramsey C (2005). OxCAL program, V.3.10 [http://c14.
arch.ox.ac/embed.php](http://c14.arch.ox.ac/embed.php)
- Bronk-Ramsey C (2009) Bayesian analysis of radiocarbon
dates. *Radiocarbon* 51:337–360
- Bunch TE, Hermes RE, Moore AMT, Kennett DJ, Weaver JC,
Wittke JH, DeCarli PS, Bischoff JL, Hillman GC, Howard
GA, Kimbel DR, Kletetschka G, Lipo CP, Sakai S, Revay
Z, West A, Firestone RB, Kennett JP (2012) Very high-
temperature impact melt products as evidence for cosmic
airbursts and impacts 12,900 years ago. *Proc Natl Acad Sci
USA* 109(28):E1903–E1912
- Bush MB, Correa-Metrio AY, Hodell DA, Brenner M, Ansel-
metti FS, Ariztegui D, Mueller AD, Curtis JH, Grzesik DA,
Burton C, Gilli A (2009) Re-evaluation of climate change
in Lowland Central America during the Last Glacial
Maximum using new sediment cores from Lake Petén Itzá,
Guatemala. In: Past climate variability in South America
and surrounding regions, developments in paleoenviron-
mental research, vol 14, Chapter 5, pp 113–128

- 1062 Carlson A (2010) What caused the Younger Dryas Cold Event?
1063 Geology 384:383–384
- 1064 Carlson AE, Clark PU, Haley BA, Klinkhammer GP, Simmons
1065 K, Brook EJ, Meissner K (2007) Geochemical proxies of
1066 North American freshwater routing during the Younger
1067 Dryas cold event. Proc Natl Acad Sci 104:6556–6561
- 1068 Choi KY, Kim Y, Chiong D, Kim YH (2014) Paleoclimate
1069 signals of Lake Hovsgol, Mongolia, over the last 19,000
1070 Years Using Authigenic Beryllium Isotopes. Radiocarbon
1071 56(3):1139–1150
- 1072 Cohen-Ofri I, Popovitz-Biro R, Weiner S (2007) Structural
1073 characterization of modern and fossilized charcoal pro-
1074 duced in natural fires as determined by using electron
1075 energy loss spectroscopy. Chem Eur J 13:2306–2310
- 1076 Cooper A, Turney C, Hughen KA, Brook BW, McDonald HG,
1077 Bradshaw JA (2015) Abrupt warming events drove Late
1078 Pleistocene Holarctic megafaunal turnover. Science
1079 349(6248):602–606
- 1080 De Mets C, Stein S (1990) Present day kinematics of the Rivera
1081 Plate and implications for tectonics in Southern Mexico.
1082 J Geophys Res 95:931–948
- 1083 Dressler BO, Reimond UW (2001) Terrestrial impact melt rocks
1084 and glasses. Earth Sci Rev 56:205–284
- 1085 Faegri K, Iversen J (1989) Textbook of pollen analysis. Black-
1086 well, London, p 287
- 1087 Firestone RB, West A, Kennett JP, Becker L, Bunch TE, Revay
1088 ZS, Schultz PH, Belgya T, Kennett DJ, Erlandson JM,
1089 Dickenson OJ (2007) Evidence for an extraterrestrial
1090 impact 12,900 years ago that contributed to the megafaunal
1091 extinctions and the Younger Dryas cooling. Proc Natl Acad
1092 Sci 104:16016–16021
- 1093 González S, Huddart D (2007) Paleoindians and megafaunal
1094 extinctions in the Basin of Mexico: the role of the 10.5 K
1095 Upper Toluca Pumice eruption. In: Grattan J, Torrence R
1096 (eds) Living under the shadow: the archaeological, cultural
1097 and environmental impact of volcanic eruptions. Left Coast
1098 Press, Walnut Creek, pp 90–106
- 1099 González S, Huddart D, Israde-Alcántara I, Dominguez-Vaz-
1100 quez G, Bischoff J (2014) Tocuila Mammoths, Basin of
1101 Mexico: Late Pleistocene–Early Holocene stratigraphy and
1102 origin of the bone assemblages. Quat Sci Rev 96:222–239
- 1103 González S, Huddart D, Israde-Alcántara I, Dominguez-Vaz-
1104 quez G, Bischoff J, Felstead NJ (2015) Paleo-Indian sites
1105 from the Basin of Mexico: new evidence from stratigraphy,
1106 tephrochronology and dating. Quat Int 363:4–19
- 1107 Harris Parks E (2016) The micromorphology of Younger Dryas-
1108 aged black mats from Nevada. Quat Res 85:94–106
- 1109 Haynes CV (2008) Younger Dryas “black mats” and the Ran-
1110 cholabrean termination in North America. Proc Natl Acad
1111 Sci 105:6520–6525
- 1112 Holliday VT (1985) Archaeological geology of the Lubbock
1113 Lake site, southern high plains of Texas. Geol Soc Am Bull
1114 96:1483–1492
- 1115 Islebe GA, Hooghiemstra H (2006) Effects of the Younger
1116 Dryas cooling event on late Quaternary montane oak forest
1117 in Costa Rica. In: Kappelle M (ed) Ecology and conser-
1118 vation of neotropical montane oak forests, vol 185. Studies
1119 in ecology. Springer, Berlin, pp 29–37
- 1120 Israde-Alcántara I, Miller WE, Garduño-Monroy VH, Barron J,
1121 Rodríguez-Pascua M (2010) Palaeoenvironmental signifi-
1122 cance of diatom and vertebrate fossils from Late Cenozoic
1123 Tectonic Basins in west-central México: a review. Quat Int
1124 219:79–94
- 1125 Israde-Alcántara I, Bischoff JL, Domínguez-Vásquez G, Li
1126 H-C, DeCarli PS, Bunch TE, Wittke JH, Weaver JC,
1127 Firestone RB, West A, Kennett JP, Mercer C, Xie S,
1128 Richman EK, Kinzie CR, Wolbach WS (2012) Evidence
1129 from central Mexico supporting the Younger Dryas
1130 extraterrestrial impact hypothesis. Proc Natl Acad Sci USA
1131 109:E738–E747
- 1132 Kennett DJ, Kennett JP, West A, West GJ, Bunch TE, Culleton
1133 BJ, Erlandson JM, Que Hee SS, Johnson JR, Mercer C,
1134 Shen F, Sellers M, Stafford TW Jr, Stich A, Weaver JC,
1135 Wittke JH, Wolbach WS (2009) Shock-synthesized
1136 hexagonal diamonds in Younger Dryas boundary sedi-
1137 ments. Proc Natl Acad Sci USA 106(31):12623–12628
- 1138 Kennett JP, Kennett DJ, Culleton BJ, Tortosa JE, Bischoff JL,
1139 Bunch TE, Daniel IR, Erlandson JM, Ferraro D, Firestone
1140 RB, Goodyear AC (2015) Bayesian chronological analyses
1141 consistent with synchronous age of 12835–12735 cal yr
1142 BP for Younger Dryas boundary on four continents. Proc
1143 Natl Acad Sci 112:4344–4353
- 1144 Kinzie CR, Hee SS, Stich A, Tague KA, Mercer C, Razink JJ,
1145 Kennett DJ, DeCarli PS, Bunch TE, Wittke JH, Israde-
1146 Alcántara I (2014) Nanodiamond-rich layer across three
1147 continents consistent with major cosmic impact at
1148 12,800 cal yr BP. J Geol 122:475–506
- 1149 Krammer K, Lange-Bertalot H (1997a) Bacillariophyceae 2/1.
1150 Teil: Naviculaceae. In: Ettl H, Gerloff J, Heynig H, Mol-
1151 lenhauer D (eds) Süßwasserflora von Mitteleuropa. Gus-
1152 tav Fisher, Stuttgart, p 876
- 1153 Krammer K, Lange-Bertalot H (1997b) Bacillariophyceae 2/2.
1154 Teil: Bacillariaceae, Epithemiaceae, Surirellaceae. In: Ettl
1155 H, Gerloff J, Heynig H, Mollenhauer D (eds) Süßwasser-
1156 flora von Mitteleuropa. Gustav Fisher, Stuttgart, p 437
- 1157 Krammer K, Lange-Bertalot H (2004) Bacillariophyceae. 2/3.
1158 Teil: Centrales, Fragilariaceae, Eunotiaceae. In: Ettl H,
1159 Gerloff J, Heynig H, Mollenhauer D (eds) Süßwasserflora
1160 von Mitteleuropa. Gustav Fisher, Stuttgart, p 598
- 1161 Kurbatov AV, Mayewski PA, Steffensen JP, West A, Kennett
1162 DJ, Kennett JP, Bunch TE, Handley M, Introne DS, Hee Q,
1163 Shane S (2010) Discovery of a nanodiamond rich layer in
1164 the Greenland ice sheet. J Glaciol 56:747–757
- 1165 LeCompte MA, Goodyear AC, Demitroff MN, Batchelor D,
1166 Vogel EK, Mooney C, Rock BN, Seidel AW (2012)
1167 Independent evaluation of conflicting microspherule
1168 results from different investigations of the Younger Dryas
1169 impact hypothesis. Proc Natl Acad Sci USA 109:E2960–
1170 E2969
- 1171 Lorenzo JL, Mirambell L (1986) Preliminary report on arche-
1172 ological and paleoenvironmental studies in the area of El
1173 Cedral, SanLuis Potosí, México. In: Bryan AL (ed) New
1174 evidence for the Pleistocene peopling of the Americas.
1175 Center for the Study of the Early Man, University of Maine,
1176 Peopling of the Americas, Symposia Series, Orono, Maine,
1177 pp 107–113
- 1178 Lozano García S, Ortega Guerrero B (1994) Palynological and
1179 magnetic susceptibility records of Lake Chalco, central
1180 Mexico. Palaeogeogr Palaeoclimatol Palaeoecol
1181 109(2–4):177–191
- 1182 Mahaney WC, Kalm V, Krinsley DH, Tricart PM, Schwartz S,
1183 Dohm J, Kim KJ, Kapran B, Milner MW, Beukens R, 1183

- 1184 Boccia S, Hancock RGV, Hart KM, Kelleher B (2010a)
 1185 Evidence from the northwestern Venezuelan Andes for
 1186 extraterrestrial impact: the black mat enigma. *Geomorphology* 116:48–57
 1187
 1188 Mahaney WC, Krinsley D, Kalm V (2010b) Evidence for a
 1189 cosmogenic origin of fired glaciofluvial beds in the north-
 1190 western Andes: correlation with experimentally heated
 1191 quartz and feldspar. *Sed Geol* 231:31–40
 1192 Mahaney WC, Keiser L, Krinsley DH, West A, Dirszowsky R,
 1193 Allen CR, Costa P (2014) Recent developments in the
 1194 analysis of the Black Mat layer and cosmic impact at
 1195 12.8 ka. *Geogr Ann Ser A Phys Geogr* 96:99–111
 1196 Meltzer DJ, Holliday VT, Cannon MD, Miller DS (2014)
 1197 Chronological evidence fails to support claim of an iso-
 1198 chronous widespread layer of dated to 12,800 years ago.
 1199 *Natl Acad Sci USA, Proc.* doi:[10.1073/pnas.1401150111](https://doi.org/10.1073/pnas.1401150111)
 1200 Mirambell L (Coordinadora) (2012) Rancho “La Amapola”,
 1201 Cedral. Un sitio arqueológico-paleontológico Pleis-
 1202 tocenico-Holoceno con restos de actividad humana.
 1203 Instituto Nacional de Antropología e Historia, México.
 1204 Serie Memorias
 1205 Mooser F (1967) Tefracronología de la Cuenca de México para
 1206 los últimos treinta mil años. *Boletín del INAH de México*
 1207 30:12–15
 1208 Morett L, Arroyo-Cabrales J, Polaco OJ (1998) Tocuila, a
 1209 remarkable mammoth site in the Basin of Mexico. *Curr Res*
 1210 *Pleistocene* 15:118–120
 1211 Ortega B, Caballero C, Lozano S, Israde I, Vilaclara G (2002)
 1212 52,000 years of environmental history in Zacapu Basin,
 1213 Michoacán, México: the magnetic record. *Earth Planet Sci*
 1214 *Lett* 202:663–675
 1215 Ortega-Guerrero B, Vazquez G, Caballero M, Israde I, Lozano-
 1216 Garcia S, Schaaf P, Torres E (2010) Late Pleistocene:
 1217 Holocene record of environmental changes in Lake Zir-
 1218 ahuen, Central Mexico. *J Paleolimnol* 44:745–760
 1219 Petaev MI, Jacobsen SB (2004) Differentiation of metal-rich
 1220 meteoritic parent bodies. Measurements of PGEs, Re, Mo,
 1221 W, and Au in meteoritic Fe–Ni metal. *Meteorit Planet Sci*
 1222 39:1685–1697
 1223 Quade J, Forester RM, Pratt WL, Carter C (1998) Black mats,
 1224 spring-fed streams, and late-glacial-age recharge in the
 1225 Southern Great Basin. *Quat Res* 49:129–148
 1226 Renssen H, Mairesse A, Goosse H, Mathiot P, Heir O, Roche
 1227 DM, Nisancioglu KH, Valdes PJ (2015) Multiple causes of
 1228 the Younger Dryas cold period. *Nat Geosci* 8:946–949
 1229 Ruiz FM, Abad AM, Bodergat P, Carbonel J, Rodriguez-Lazaro
 1230 ML, Gonzalez-Regalado A, Toscano EX, Garcia J Prenda
 (2013) Freshwater ostracods as environmental tracers. *Int J*
 1231 *Environ Sci Technol* 2013(10):1115–1128
 1232
 1233 Scott AC, Pinter N, Collinson ME, Hardiman M, Anderson RS,
 1234 Brain AP, Smith SY, Marone F, Stampanoni M (2010)
 1235 Fungus, no comet or catastrophe, accounts for carbona-
 1236 ceous spherules in the Younger Dryas “impact layer”.
 1237 *Geophys Res Lett* 37:14302–14307
 1238 Siebe C, Schaaf P, Urrutia-Fucugauchi J (1999) Mammoth
 1239 bones embedded in a late Pleistocene Lahar from Popo-
 1240 catépetl volcano, near Tocuila, central Mexico. *Bull Geol*
 1241 *Soc Am* 111:1550–1562
 1242 Suter M, Quintero O, Johnson J (1992) Active faults and state of
 1243 stress in the central part of the Mexican Volcanic Belt: the
 1244 Venta de Bravo fault. *J Geophys Res* 97(B8):983–993
 1245 Suter M, Lopez Martinez M, Quintero O, Carillo M (2001)
 1246 Trans-Mexican Volcanic Belt. *Bull Geol Soc Am*
 1247 113:693–703
 1248 Tarasov L, Peltier WR (2005) Arctic freshwater forcing of the
 1249 Younger Dryas cold reversal. *Nature* 435:662–665
 1250 Tian H, Schryvers D, Claeys P (2011) Nanodiamonds do not
 1251 provide unique evidence for a Younger Dryas impact. *Proc*
 1252 *Natl Acad Sci USA* 108:40–44
 1253 Torres-Rodríguez E, Lozano-García S, Figueroa-Rangel BL,
 1254 Ortega-Guerrero B, Vázquez-Castro G (2012) Cambio
 1255 ambiental y respuestas de la vegetación de los últimos
 1256 17,000 años en el centro de México: el registro del lago de
 1257 Zirahuén. *Revista Mexicana de Ciencias Geológicas*
 1258 29(3):764–768
 1259 Wittke CJ, Weaver JC, Bunch TE, Kennett JP, Kennett DG,
 1260 Moore AM, Hillman GC, Tankersley KB, Goodyear AC,
 1261 Moore C, Daniel Jr IR, Ray JH, Lopinot N, Ferraro D,
 1262 Israde-Alcántara I, Bischoff JL, DeCarli P, Hermes R,
 1263 Kloosterman J, Revay Z, Howard G, Kimbel D, Kle-
 1264 tetschka G, Nabelek L, Lipo C, Sakai S, West A, Firestone
 1265 R (2013) Evidence for deposition of 10 million tonnes of
 1266 impact spherules across four continents 12,800 yr ago.
 1267 *June 2013.* www.pnas.org/cgi/doi/10.1073/pnas.1301760110. ISSN: 0027-8424
 1268
 1269 Zárate del Valle P, Dörfler W, Albrechts C, Nelle O, Israde-
 1270 Alcántara I (2014) CHAPHOLO: Paleolimnological eval-
 1271 uation of Lake Chapala (Western Mexico) During the Past
 1272 10,000 Years (CONACYT CB2011, Grant 168685, in
 1273 Progress). PHASE I: Drilling Campaign. AGU fall meet-
 1274 ing. 2014 Abstract ID: 13748 final paper Number: PP31A-
 1275 1115